Chemical Science

ROYAL SOCIETY OF CHEMISTRY

EDGE ARTICLE

View Article Online
View Journal | View Issue



Cite this: *Chem. Sci.*, 2024, **15**, 12369

All publication charges for this article have been paid for by the Royal Society of Chemistry

# Understanding the role of supported Rh atoms and clusters during hydroformylation and CO hydrogenation reactions with *in situ*/*operando* XAS and DRIFT spectroscopy†

Bidyut Bikash Sarma, *[abc] Dominik Neukum, [b] Dmitry E. Doronkin, [ab] Ajai Raj Lakshmi Nilayam, [d] Lorena Baumgarten, [ab] Bärbel Krause [e] and Jan-Dierk Grunwaldt [ab]

Supported Rh single-atoms and clusters on $CeO_2$, MgO, and $ZrO_2$ were investigated as catalysts for hydroformylation of ethylene to propionaldehyde and CO hydrogenation to methanol/ethanol with *in situ*/*operando* diffuse reflectance infrared Fourier transform spectroscopy (DRIFTS) and X-ray absorption spectroscopy (XAS). Under hydroformylation reaction conditions, *operando* spectroscopic investigations unravel the presence of both single atoms and clusters and detected at first propanal and then methanol. We find that the formation of methanol is associated with CO hydrogenation over Rh clusters which was further confirmed under CO hydrogenation conditions at elevated pressure. The activity of catalysts synthesized *via* a precipitation (PP) method over various supports towards the hydroformylation reaction follows the order: $Rh/ZrO_2$ > $Rh/CeO_2$ > Rh/MgO. Comparing $Rh/CeO_2$ catalysts synthesized *via* different methods, catalysts prepared by flame spray pyrolysis (FSP) showed catalytic activity for the hydroformylation reaction at lower temperatures (413 K), whereas catalysts prepared by wet impregnation (WI) showed the highest stability. These results not only provide fundamental insights into the atomistic level of industrially relevant reactions but also pave the way for a rational design of new catalysts in the future.

Received 2nd May 2024
Accepted 29th June 2024

DOI: 10.1039/d4sc02907k

rsc.li/chemical-science



## Introduction

The hydroformylation (HF) reaction, an industrially demanding reaction for producing aldehydes *via* the reaction of olefin and synthesis gas, is predominantly catalyzed by Rh molecular catalysts.[1,2] On the other hand, higher alcohol synthesis (HAS)[3–5] proceeds only in the presence of synthesis gas and is largely catalyzed by Rh solid catalysts.[5–7] Both reactions follow rather similar pathways *via* C–CO coupling reactions and yet the products are different. Recent studies show that Rh single-atom catalysts (SACs)[8–10] can be promising alternatives for heterogeneously catalyzed hydroformylation reactions[11,12] where the C–CO coupling reaction occurs like in conventional homogeneous Rh-phosphine complexes. Therefore, SACs are considered analogous to molecular catalysts.[13,14] The tunable local environment around the supported single atom makes it particularly attractive to investigate how the C–CO coupling reaction takes place. A recent example shows that Rh-$WO_x$ pair site catalysts can boost the activity for gas phase hydroformylation reactions.[15] However, SACs are also prone to agglomeration due to their high surface energy particularly in a highly reductive environment.[16,17] Several reports claimed that Rh SACs stabilized by ionic liquids,[18] functionalized with an alkyl chain over a solid support,[19] synthesized by tuning surface deficiencies,[20] and even with strong metal–support cooperativity[21,22] show superior stability. Zhao *et al.* observed redispersion of $Rh^0$ clusters inside zeolite MFI to Rh single atoms and, ultimately, the formation of $Rh^+(CO)_2$ during hydroformylation of ethylene at 50 °C, which shows that the dynamic structural change plays a vital role under operating conditions.[23]

In the absence of an olefin, CO hydrogenation to higher alcohols ($C_{2+}$) over Rh catalysts[7,24,25] is a promising route since the synthesis gas mixture can be obtained from various

[a]*Institute for Chemical Technology and Polymer Chemistry, Karlsruhe Institute of Technology (KIT), Engesserstraße 20, 76131 Karlsruhe, Germany*

[b]*Institute of Catalysis Research and Technology, KIT, Hermann-von Helmholtz Platz 1, 76344 Eggenstein-Leopoldshafen, Germany*

[c]*Laboratoire de Chimie de Coordination (LCC), CNRS, Université de Toulouse, INPT, 205 route de Narbonne, 31077 Toulouse Cedex 4, France*

[d]*Institute of Nanotechnology, KIT, Hermann-von-Helmholtz Platz 1, 76344 Eggenstein-Leopoldshafen, Germany*

[e]*Institut für Photonenforschung und Synchrotronstrahlung (IPS), KIT, Hermann-von-Helmholtz Platz 1, D-76021 Karlsruhe, Germany. E-mail: bidyut-bikash.sarma@lcc-toulouse.fr; bidyutbikash.sarma@toulouse-inp.fr*

† Electronic supplementary information (ESI) available. See DOI: https://doi.org/10.1039/d4sc02907k

processes based on renewable resources such as biomass conversion,[26] $CO_2$ valorization,[27] dry-reforming of $CO_2$ with $CH_4$,[28] electrochemical conversion of $CO_2$,[29] photochemical conversion of $CO_2$,[30] conversion of plastic waste,[31] and many others.[32] However, until today, there has been no suitable catalyst that can achieve the desired activity and selectivity which are required for industrial scale production.[33] Therefore, it is extremely important to know the effect of Rh nuclearity,[24,34] support,[35] adsorbate–adsorbate interaction,[36] promoters,[32,33] morphology,[25] and particle size.[37] Cu-based catalysts are also promising alternatives for CO hydrogenation to higher alcohols; however, they compete with methanol synthesis and require promoters of alkali, transition, and rare-earth metals to produce higher alcohols as selective products.[38–40] The limitation of using other transition metals such as Co is that it catalyzes the competing Fischer–Tropsch process.[41]

A typical homogeneous HF reaction follows the classical Heck–Breslow mechanism[42,43] and usually proceeds *via* several steps such as (a) ligand dissociation from the complex, (b) olefin coordination, (c) alkyl formation *via* hydride insertion, (d) CO insertion, (e) $H_2$ oxidative addition and (f) reductive elimination. On the other hand, HAS involves (a) CO dissociation, (b) carbon–carbon bond formation, (c) CO insertion and (d) stepwise hydrogenation to the alcohol.[33,44] While in the HF reaction, all the steps can potentially occur over monometallic Rh, in HAS, synergetic effects between two neighbouring sites are likely required for C–C bond formation and CO insertion steps. For monometallic catalysts, the $M^0$ state is assumed to promote the C–C chain growth during HAS whereas $M^{\delta+}$ is responsible for CO insertion like in the classical HF reaction.[33,45]

This brings us to the question of whether Rh SACs can be active for both types of reactions as Rh exhibits a positive charge, and in a reductive environment, $Rh^0$ has been observed.[5] There have been many reports where the co-existence of SACs and small clusters was detected simultaneously under *in situ* conditions such as propane dehydrogenation,[46] dry-reforming of methane,[47,48] or $CO_2$ hydrogenation.[49,50] On the other hand, it is well known that Rh forms $Rh(CO)_2^+$-carbonyls in the presence of CO due to the strong interaction of CO with Rh.[51] In many of these catalytic processes, the presence of two species led to two different reaction pathways and hence two different products were observed. A recent study by Wu *et al.* claimed that the dynamic evolution of Rh single atoms to clusters over $CeO_2$ led to good activity for CO hydrogenation to ethanol, where the presence of Rh single atoms and clusters was found during the catalytic activity test.[34]

To understand these two reactions in detail, which can occur in parallel, we have synthesized Rh SACs and cluster catalysts over various supports ($CeO_2$, MgO, and $ZrO_2$) *via* precipitation,[16] atom trapping,[52,53] pyrolysis of molecular complexes[54] and flame spray pyrolysis (FSP).[55] These supports are chosen due to their variable acidity, reducibility, and, most importantly, variation in reactivity during the catalytic HF reaction as reported in the literature.[9] The as-synthesized catalysts were characterized *ex situ* by various state-of-the-art characterization methods and the dynamic behaviour[56] of Rh catalysts was tracked by *in situ* X-ray absorption spectroscopy (XAS)[57] and diffuse reflectance Fourier transform infrared spectroscopy (DRIFTS).[16] The products of the two reactions, (a) hydroformylation of ethylene to propanal and (b) CO hydrogenation to methanol/ethanol were monitored using an online mass spectrometer (MS).

## Results and discussion

### Synthesis and characterization of catalysts

The Rh catalysts synthesized *via* different routes have different metal contents in the range between 0.8 and 1.5 wt% as confirmed by the inductively coupled plasma optical emission spectroscopy (ICP-OES) analysis. A plot of BET surface area as a function of metal content in the catalysts is shown in Fig. S1 of the ESI.† The surface area varies greatly depending on the support and synthesis procedure. For example, $Rh/CeO_2$ catalysts synthesized *via* FSP showed the highest specific surface area (133 $m^2\ g^{-1}$) in comparison to the one synthesized by wet impregnation (56 $m^2\ g^{-1}$) or precipitation methods (93 $m^2\ g^{-1}$). This is due to the fast quenching of the resulting solid synthesized by the FSP method which minimizes the particle growth, as explained elsewhere.[55] Among the catalysts prepared over different supports ($CeO_2$, $ZrO_2$ and MgO), $ZrO_2$ (synthesized by the precipitation method) showed the highest specific surface area of 201 $m^2\ g^{-1}$, which makes it attractive for application in catalysis.

The powder X-ray diffraction (XRD) patterns of the as-synthesized catalysts showed highly crystalline structures (Fig. S2–S7 in ESI†) in all cases. There is no Rh reflection (at $2\theta = 40°$) observed, confirming the high dispersion of Rh over different supports. Even when the content of Rh is increased from 0.6 wt% to 5 wt% over the $CeO_2$ support, we did not observe any reflection associated with Rh metal or $RhO_x$ clusters as shown in Fig. S2.† The FSP method was also successful in preventing the formation of Rh nano-particles with long-range order (Fig. S3†), as also reported in the literature for other metals.[58–60] Aberration-corrected ($C_s$) high-angle annular dark-field (HAADF) scanning transmission electron microscopy (STEM) was used to visualize the nuclearity of Rh in the as-synthesized state of the catalysts over different supports. The images and the corresponding Energy Dispersive X-ray (EDX) maps are shown in Fig. 1 and in Fig. S8–S10.† The EDX maps confirm that Rh is uniformly distributed in all the catalysts except the Rh catalyst supported over $CeO_2$ synthesized by the pyrolysis method. In this case, RhP was formed, which showed nano-particle formation. The presence of some clusters (<2 nm) in the FSP synthesized catalyst cannot be entirely ignored, as observed in the EDX maps (Fig. S8†).

We further conducted X-ray absorption spectroscopy (XAS) to elucidate the local structure of the Rh catalysts as shown in Fig. 2. The extended X-ray absorption fine structure analysis (EXAFS) showed that Rh species over $CeO_2$, $ZrO_2$, and MgO are highly dispersed with Rh–O as the first coordination shell (without any Rh–Rh scattering) whereas the $RhP/CeO_2$ catalyst exhibits predominantly the Rh–Rh shell as shown in Fig. 2(a). The X-ray absorption near edge structure (XANES) spectra at the Rh K-edge showed that Rh is in an oxidation state of +3 over $CeO_2$, $ZrO_2$ and MgO and in a partially reduced state in the RhP/

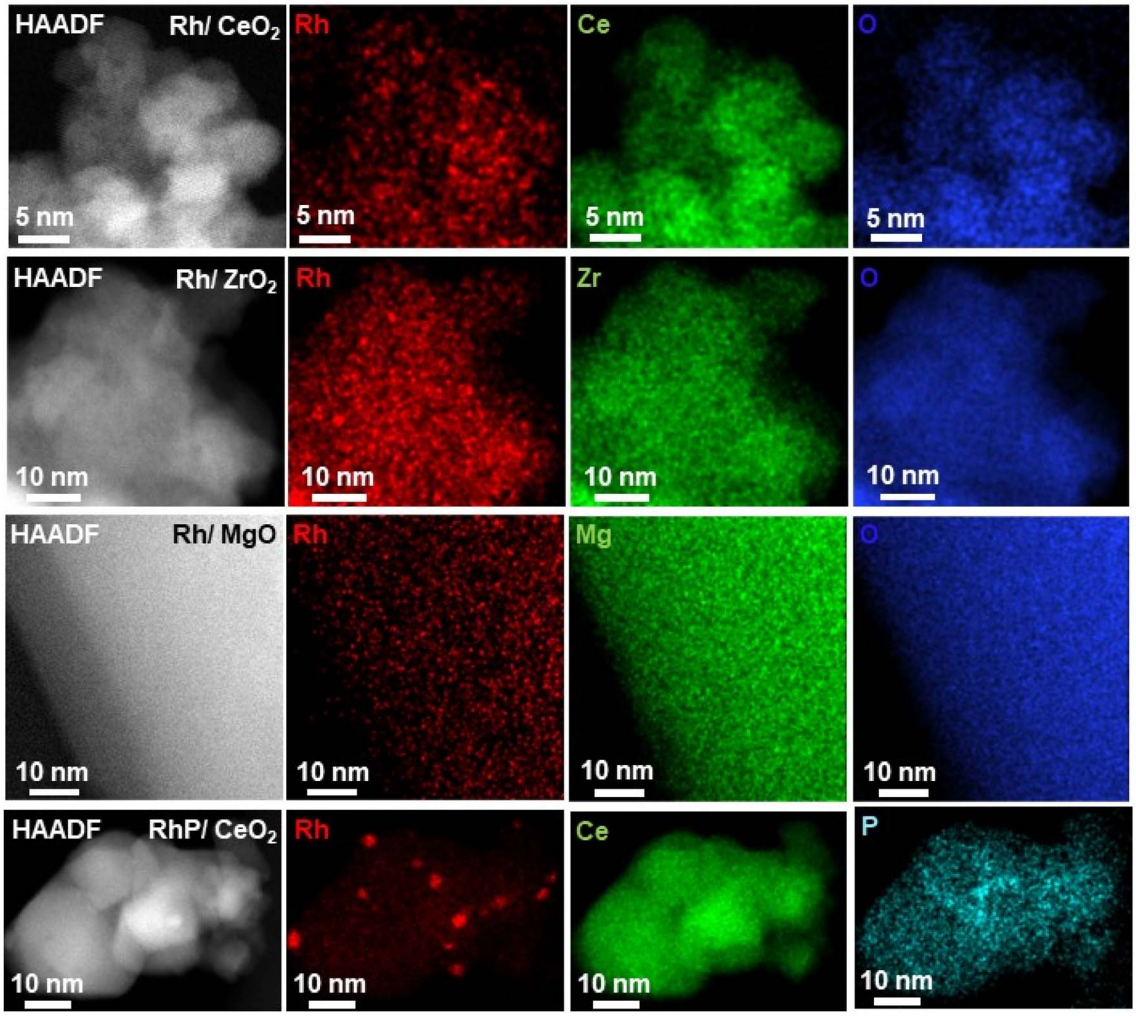


Fig. 1 HAADF-STEM images of Rh catalysts and the corresponding EDX maps. $Rh/CeO_2$, $Rh/ZrO_2$, Rh/MgO are synthesized *via* the precipitation method, and $RhP/CeO_2$ is synthesized *via* the pyrolysis route.

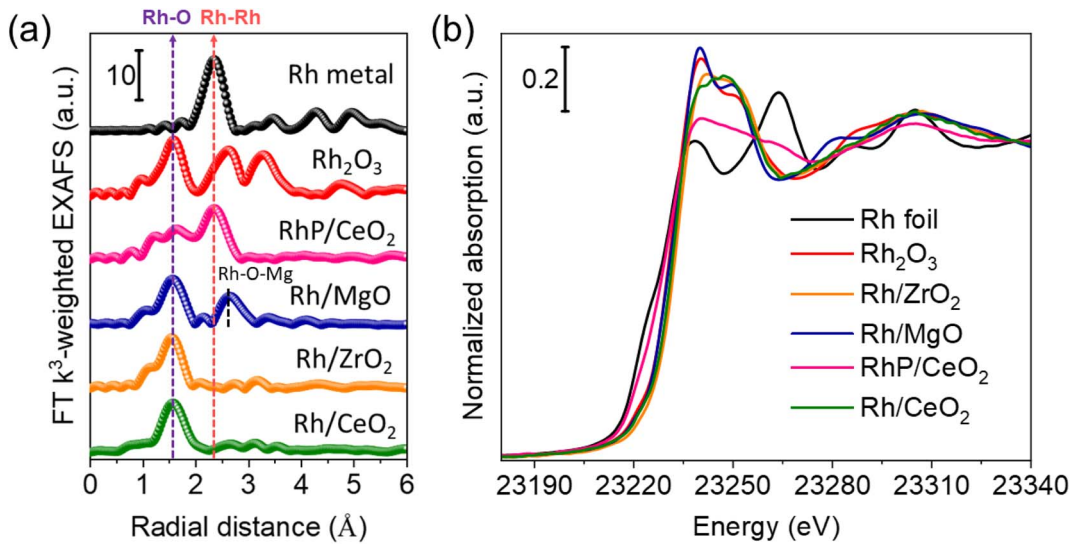


Fig. 2 (a) Fourier transform of the $k^3$-weighted EXAFS spectra and (b) XANES spectra at the Rh K-edge of the Rh catalysts supported over $CeO_2$, $ZrO_2$, and MgO. $Rh_2O_3$ and Rh foil are shown as references for comparison.

$CeO_2$ catalyst as shown in Fig. 2(b). The spectra of Rh catalysts synthesized over ceria with various methods are shown in ESI Fig. S11,† and the corresponding free parameters derived from the fit are shown in Table S2.† The X-ray photoelectron spectroscopy (XPS) investigation further supported the results obtained from XAS. All the catalysts except $RhP/CeO_2$ contain $Rh^{III}$ as the predominant species on the surface as shown in Fig. S12 of the ESI.† The components present and their percentages are shown in Table S2.†

XAS[57] is an averaging technique over all species present and has certain limitations when used on heterogeneous samples. For example, over the oxide-supported catalyst, EXAFS cannot distinguish between single site and clusters of a few atoms as explained by Finzel *et al.*[61] Therefore, as a complementary technique, we carried out diffuse reflectance Fourier transform infrared spectroscopy (DRIFTS) investigations with CO as a probe molecule to elucidate the nuclearity of the Rh catalysts synthesized over different supports as shown in Fig. 3. CO adsorbed on Rh shows characteristic symmetric and anti-symmetric CO vibrational frequencies of single site $Rh^{I}(CO)_2$ in the range of 2070–2090 $cm^{-1}$ and 2000–2020 $cm^{-1}$ respectively.[16,49,62,63] $Rh/CeO_2$ synthesized *via* precipitation (PP), flame spray pyrolysis (FSP) and wet impregnation (WI) exhibit Rh single sites as the predominant species as shown in Fig. 3(a), (d) and (e) respectively. Similarly, $Rh/ZrO_2$ (PP) also showed the presence of symmetrical and asymmetrical CO vibrational frequencies at 2078 and 2007 $cm^{-1}$ respectively.[64] On the other hand, the $RhP/CeO_2$ catalyst synthesized *via* the pyrolysis method showed the presence of CO adsorption over the Rh clusters in the lower frequency region (1850–1950 $cm^{-1}$)[16] as shown in Fig. 3(c). The spectra are also shown on the logarithmic scale in Fig. S13.† These results are in agreement with the TEM observations (Fig. 1), which indicate the presence of Rh clusters as $RhP/CeO_2$. The DRIFT spectra of $Rh/CeO_2$ (5 wt%) with adsorbed CO showed various features (2126, 2035 $cm^{-1}$), which can be attributed to the weakly adsorbed CO over $Rh^{3+}$ or $Rh^{2+}$ species present in the form of $RhO_x$ clusters.[23] Upon flowing Ar, two distinct CO absorption frequencies at 2023 and 2092 $cm^{-1}$ were observed, as shown in Fig. S14,† which we believe arise from the fraction of Rh single atoms present in this high loading catalyst. Moreover, the presence of a broad CO adsorption peak between 1850 and 1900 $cm^{-1}$ (Fig. S14†) infers the presence of Rh clusters in this catalyst. The Rh/MgO catalyst did not show any CO vibrational frequencies in the range 1800–2100 $cm^{-1}$, which indicates that Rh supported on MgO is coordinatively saturated as also found previously.[9,65] The CO

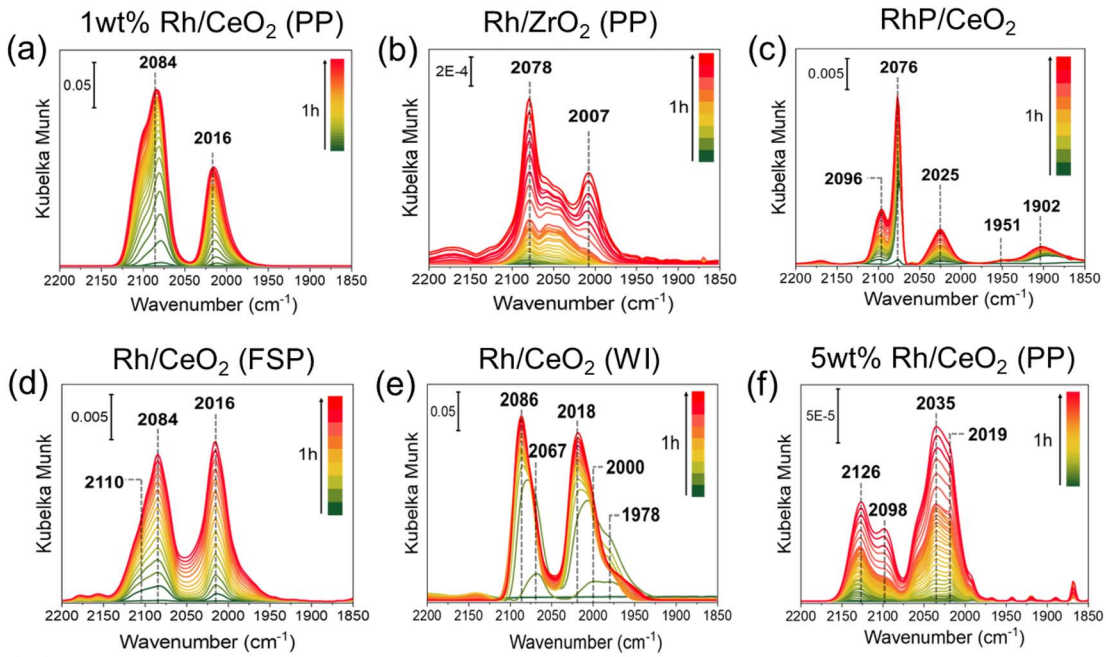


(g)

| CO adsorption frequency ($cm^{-1}$) | Assignments | CO adsorption frequency ($cm^{-1}$) | Assignments |
|---|---|---|---|
| 2084 ($\nu_s$), 2016 ($\nu_{as}$) | $Rh(CO)_2/CeO_2$ | 2110 | $Rh^{+}(CO)/CeO_2$ |
| 2078 ($\nu_s$), 2007 ($\nu_{as}$) | $Rh(CO)_2/ZrO_2$ | 2046 | $Rh_2(CO)/CeO_2$ |
| 2098 ($\nu_s$), 2035 ($\nu_{as}$) | $Rh^{+}(CO)_2/CeO_2$ | 1902 | $Rh_2(CO)/CeO_2$ |
| 2126 | $Rh^{3+}(CO)/CeO_2$ | 2150-2180 | Gas phase CO |

Fig. 3 CO-DRIFTS spectra at room temperature over various Rh catalysts. (a) $Rh/CeO_2$ (PP), (b) $Rh/ZrO_2$ (PP), (c) $RhP/CeO_2$, (d) $Rh/CeO_2$ (FSP), (e) $Rh/CeO_2$ (WI), and (f) 5 wt% $Rh/CeO_2$ (PP). (g) Table of CO absorption frequency with assignments of Rh species. PP: precipitation, FSP: flame spray pyrolysis, and WI: wet impregnation. $\nu_s$ and $\nu_{as}$ stands for symmetric and anti-symmetric CO vibrational frequencies. The green to red color bar represents the experiment over 1 hour at room temperature.

absorption frequencies of Rh catalysts over various supports and their assignments are shown in Fig. 3(g) as well as in Table S4 of the ESI.†

### *In situ* XAS investigations

In order to understand the electronic state of Rh under operating conditions, we further carried out *in situ* XAS studies at the Rh K-edge for hydroformylation of ethylene (experimental setup is shown in S15 of the ESI†). The catalysts were exposed to a mixture of a 1 : 1 : 1 ratio of ethylene : CO : $H_2$ while heating from room temperature to 573 K (2 K $min^{-1}$ and 30 min dwell time) at atmospheric pressure with a total flow of 40 mL $min^{-1}$. The gas mixture at the outlet was monitored with an online mass spectrometer. The temperature-dependent *in situ* XANES spectra were collected continuously at the Rh K-edge from room temperature to 573 K in the presence of the reaction mixture as shown in Fig. 4(a)–(d). All Rh catalysts were reduced under HF conditions with a change in the oxidation state of Rh from $Rh^{3+}$ to $Rh^0$. Linear combination analysis (LCA) was used to derive the oxidized and reduced components during the reaction as shown in Fig. 4 (e)–(h). The trend of the reduction temperature from the highest to the lowest follows the order of Rh/MgO > $Rh/ZrO_2$ > $Rh/CeO_2$ > $RhP/CeO_2$. However, the catalytic activity does not follow the same trend. Both in $Rh/CeO_2$ and $Rh/ZrO_2$, we observed propanal at around a temperature of 500 K, which is the product formed *via* the HF reaction as shown in Fig. 4(i) and (j). At this stage, almost 80–90% of the Rh species are already reduced which indicates the possible involvement of clusters during catalysis. Interestingly, when all the Rh is reduced, methanol is detected in the MS. This indicates that when Rh forms clusters, the pathway for CO hydrogenation is enhanced as also shown by Wu *et al.*[34] This is supported by our catalytic test over the $RhP/CeO_2$ catalyst which contains a significant fraction of Rh clusters, for which formation of methanol was detected almost parallel to the formation of propanal (Fig. 4(l)). Rh/MgO did not show any activity even in the presence of reduced rhodium, which indicates that the basic support does not promote HF or methanol formation. Among the $Rh/CeO_2$ catalysts, Rh synthesized by FSP showed catalytic activity at a lower temperature (*ca.* 410 K) compared to the catalysts synthesized by precipitation or wet impregnation methods, as shown in Fig. S16 of the ESI.† This might be due to better accessibility of the Rh atoms deposited on high surface area $CeO_2$ when synthesized *via* the FSP method.[55]

In order to find the origin of methanol formation, we further carried out the reaction in the absence of ethylene (CO : $H_2$ of 1 : 1) in a quartz capillary micro-reactor at 10 bar pressure in the temperature range of RT-573 K. The temperature dependent

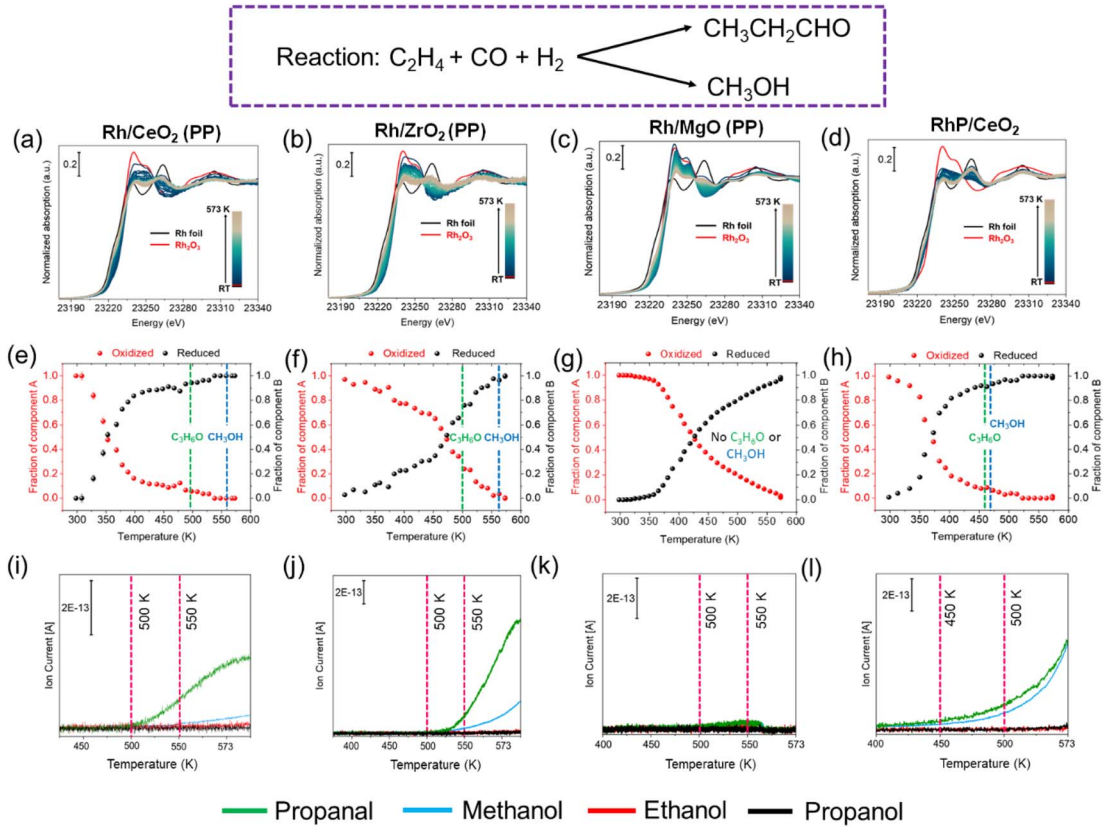


Fig. 4 *In situ* XANES spectra at the Rh K-edge of catalysts prepared over different supports ((a)–(d)), the fraction of components (oxidized and reduced) derived from linear combination fitting ((e)–(h)) during the hydroformylation reaction of ethylene, and selectivity of different products monitored using an online mass spectrometer (i)–(l). The dotted lines are a guide to the eye. PP stands for precipitation. Reaction conditions: 25 mg catalysts, 1 : 1 : 1 mixture of ethylene : CO : $H_2$, $T$ = RT-573 K (ramp rate 2 K $min^{-1}$), $P$ = 1 bar, flow rate: 40 mL $min^{-1}$.

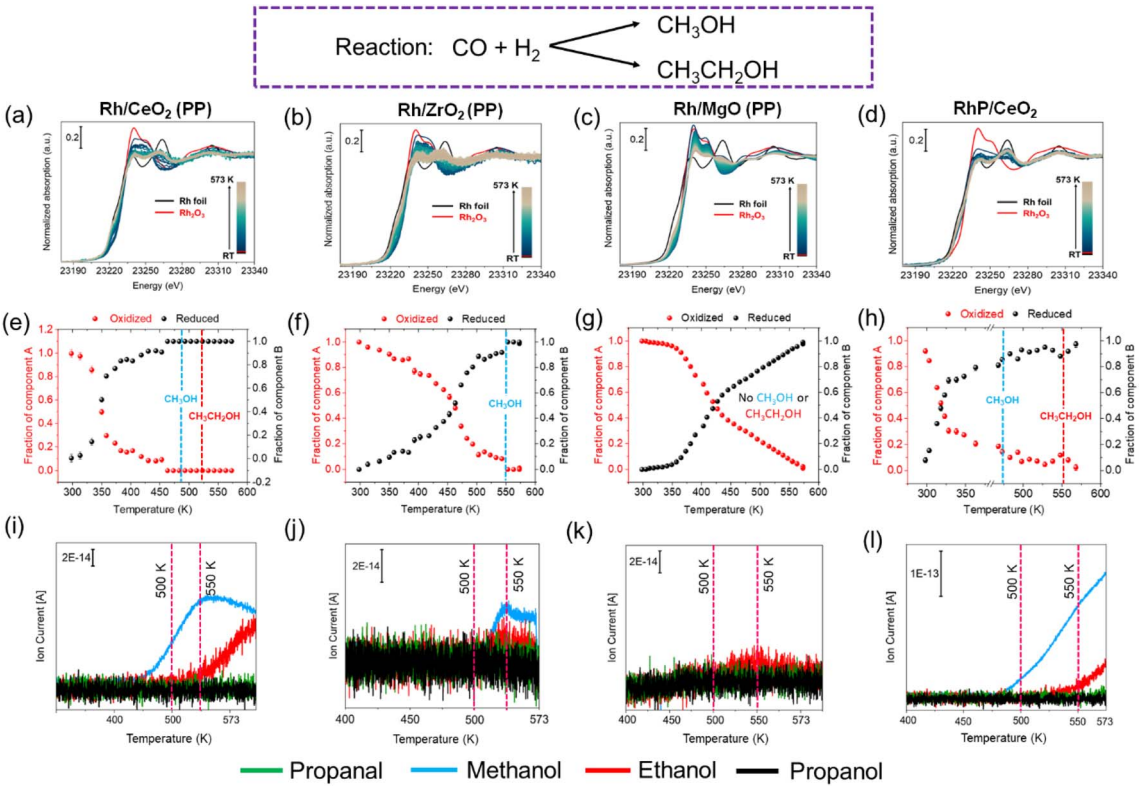


Fig. 5 *In situ* XANES spectra at the Rh K-edge of catalysts prepared over different supports ((a)–(d)), the fraction of components (oxidized and reduced) derived from linear combination fitting ((e)–(h)) during CO hydrogenation, and selectivity of different products monitored using an online mass spectrometer (i)–(l). The dotted lines are a guide to the eye. PP stands for precipitation. Reaction conditions: 25 mg catalysts, 1 : 1 mixture of CO : $H_2$, $T$ = RT-573 K (ramp rate 2 K $min^{-1}$), $P$ = 10 bar, flow rate: 40 mL $min^{-1}$.

XANES spectra and the linear combination analysis of the oxidized and reduced components during the reaction are shown in Fig. 5. The mass spectrometer (MS) detected both methanol and ethanol over $Rh/CeO_2$ synthesized *via* the precipitation method (Fig. 5(i)). This further indicates that the nuclearity of Rh plays a crucial role in obtaining methanol and ethanol products as previously reported.[24,34] The $Rh/ZrO_2$ catalyst showed only methanol in the product stream and no ethanol was observed. Rh/MgO did not show any activity as was also the case for the HF reaction. $RhP/CeO_2$ showed initially only methanol, and ethanol was only observed at higher temperatures (550 K) when a significant portion of $Rh^0$ formed. The Fourier transformed $k^3$-weighted EXAFS spectra after the HF reaction and CO hydrogenation reaction are shown in Fig. S17 of the ESI.† The predominant presence of the Rh–Rh shell indicates that most of the catalysts were reduced completely at the end of the reaction except Rh/MgO and $Rh/ZrO_2$, which showed a significant proportion of the oxidic species (presence of the Rh–O shell). We further carried out fitting of the Rh–Rh shell to calculate the coordination number of Rh in the spent catalysts. The fits and the free parameters are shown in ESI Fig. S18 and in Table S5.† The coordination numbers obtained from the fits are in the range between 1 and 6. Nevertheless, such low coordination values indicate that the size of the reduced Rh species is extremely small.[66,67] To further confirm whether the concentration of Rh plays a significant role during the reaction, we have conducted the CO hydrogenation reaction over $Rh/CeO_2$ with three different Rh loadings (1.1, 2.2 and 4.5 wt%). The results are shown in Fig. S19 of the ESI.† The catalytic results indicate that upon increasing Rh content over the $CeO_2$ support, the formation of methanol and ethanol is enhanced. 4.5 wt% $Rh/CeO_2$ showed the formation of methanol and ethanol simultaneously like the $RhP/CeO_2$ catalyst, which indicates that for a highly loaded sample, Rh easily forms nanoparticles which can promote the C–CO coupling reaction. These results further signify the role of clusters during HF and CO hydrogenation reactions.

Based on our results, three summary points can be hypothesized for the reaction mechanism. (a) Rh single atom catalysts form the active center upon treatment with syngas and actively take part in the hydroformylation reaction, (b) when Rh clusters are formed, it mainly favors methanol synthesis, and (c) for ethanol formation, both atoms and clusters participate during the reaction as the CO insertion step requires $Rh^{\delta+}$ species for C–C chain propagation. These points are summarized in Fig. S20 of the ESI.†

### *In situ* DRIFTS investigations

In order to investigate the change in the state of Rh, we carried out DRIFTS experiments under various conditions, as shown in

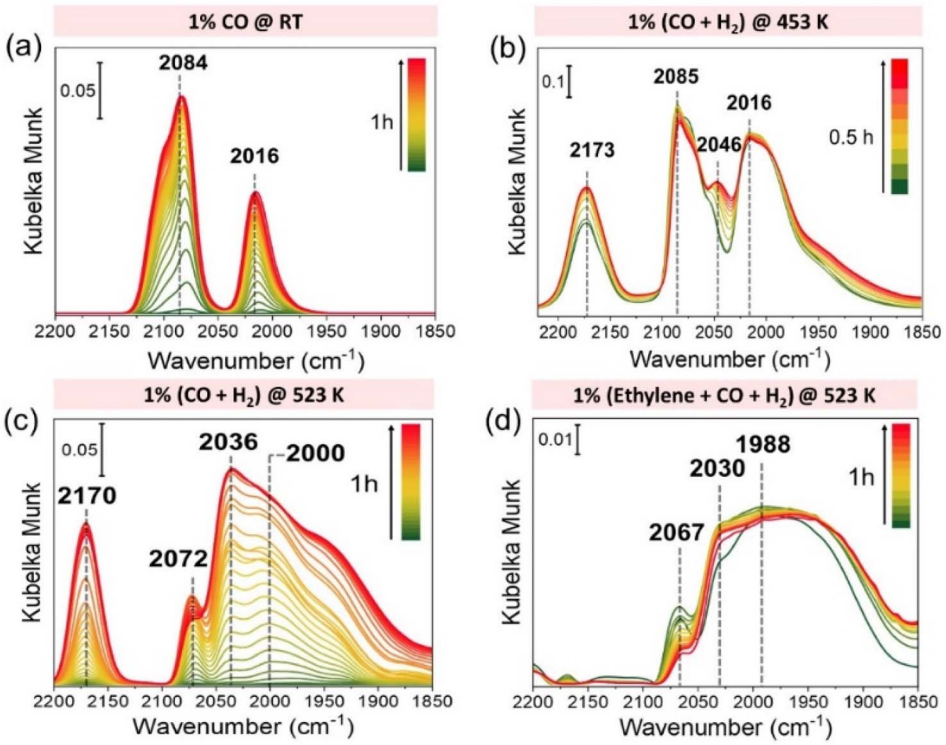


Fig. 6 *In situ* DRIFTS spectra collected for 1 hour under various conditions of the catalyst $Rh/CeO_2$ synthesized *via* precipitation method. (a) 1% CO at room temperature, (b) 1% ($CO + H_2$) at 453 K, (c) 1% ($CO + H_2$) at 523 K and (d) 1% (ethylene + $CO + H_2$) at 523 K.

Fig. 6. As discussed before, at room temperature $Rh/CeO_2$ showed CO vibrational frequencies at 2084 and 2016 $cm^{-1}$ that correspond to symmetrical and anti-symmetrical vibrational modes of CO of $Rh^I(CO)_2$ species. The change in the state of Rh is already visible at 453 K under 1% ($CO + H_2$) as a new CO vibrational frequency appears at 2046 $cm^{-1}$ (Fig. 6(b)), which corresponds to CO adsorbed on Rh clusters. Upon increasing the temperature to 523 K, clusters of Rh formed and an additional feature at 2036 $cm^{-1}$ was observed (Fig. 6(c)), which we believe to occur due to the formation of Rh(CO)H species as reported in the literature.[37] This trend continued when ethylene was introduced to the reaction mixture. However, even under such a reductive atmosphere, there is still the presence of isolated Rh species (2030 $cm^{-1}$) as shown in Fig. 6(d). These results correlate with the *in situ* XAS studies and further hint that Rh atoms and clusters formed under reaction conditions play a crucial role during the HF reaction. Additionally, we carried out DRIFTS experiments on the $Rh/CeO_2$ catalyst synthesized *via* the wet impregnation method, which showed higher stability based on our *in situ* XAS studies (Fig. S16(c)†). The DRIFTS results showed no obvious formation of clusters, unlike for the catalyst synthesized *via* the precipitation method, as shown in Fig. S21 of the ESI.† A comparison of the $H_2$-temperature programmed reduction (TPR) profile and the DRIFT spectra collected at 453 K with the catalyst prepared over various supports ($CeO_2$, $ZrO_2$, and MgO) is shown in Fig. S23 of the ESI.† The results showed that based on the support, Rh exhibits different reduction temperatures, and it follows the order of $Rh/CeO_2 < Rh/ZrO_2 < Rh/MgO$. The DRIFT spectra recorded at 453 K under $CO + H_2$ indicated that $Rh/ZrO_2$ did not show any Rh cluster formation. On the other hand, Rh/MgO did not show any feature regarding CO adsorption, which infers that Rh is not easily available on the surface of MgO and may be located in the highly coordinated bulk environment.

## Conclusions

In conclusion, we have found that highly dispersed Rh catalysts supported over $CeO_2$, $ZrO_2$, and MgO showed co-existence of supported single Rh atoms and clusters under conditions of HF of ethylene and CO hydrogenation reactions. The *in situ* XAS studies infer the formation of reduced Rh particles/clusters while both propanal and methanol were observed during the HF reaction. In addition, the *in situ* DRIFTS studies showed vibrational frequencies of CO adsorbed over Rh atoms and clusters under reaction conditions, which further supports that such unprecedented reactivity might have occurred due to the presence of both species. The formation of a significant amount of ethanol was observed during the CO hydrogenation reaction over the $RhP/CeO_2$ catalyst, which also showed the presence of nano-particles (>2 nm) already in the as-synthesized catalyst. Moreover, by increasing the concentration of Rh from 1.1 wt% to 4.5 wt% over the $CeO_2$ support, we observed the CO hydrogenation reaction at a relatively low temperature. This indicates that a certain size of Rh nano-particles is important to promote the C–C coupling reaction during higher alcohol synthesis.

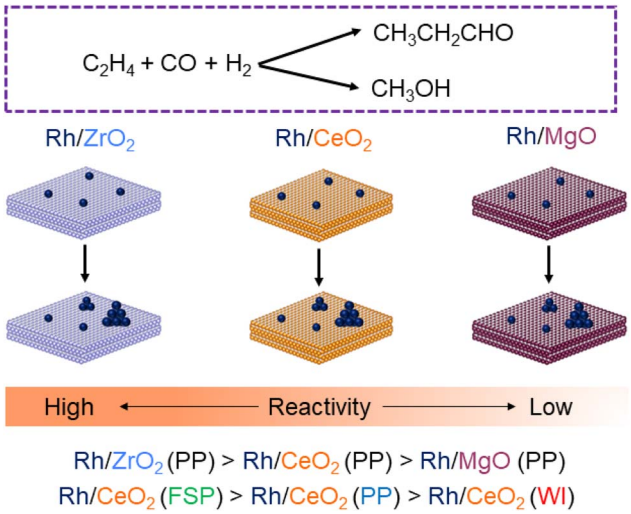


Fig. 7 Summary of reactivity towards the hydroformylation reaction of ethylene with supported Rh catalysts on $CeO_2$, $ZrO_2$, and MgO. PP, FSP, and WI stand for precipitation, flame spray pyrolysis, and wetness impregnation, respectively.

Comparisons of catalytic activity over various supports showed that acidic supports, such as $ZrO_2$, promote the hydroformylation reaction, whereas basic supports, such as MgO, result in negligible catalytic activity. The varying reactivity towards hydroformylation of ethylene is dependent on the preparation method and support, as summarized in Fig. 7. Among the catalysts synthesized over $CeO_2$ with various methods, catalysts prepared *via* flame spray pyrolysis showed activity at low temperatures which indicates that the method of preparation plays a vital role during the reaction. This study will pave the way for further development of catalysts for such an industrially relevant reaction. In the future, we plan to investigate the CO insertion mechanism of the two reactions in more detail by introducing promoters and extending the reactions over further industrially relevant supports.

## Data availability

Data supporting the article (experimental protocols, XRD, XPS, BET, and TPR results) are available in the ESI.† The raw data can be provided upon request to the corresponding author.

## Author contributions

BBS: conceptualization; investigation, data curation & formal analysis (catalyst preparation & catalytic testing, including *in situ* XAS and DRIFTS); formal analysis (XAS, DRIFT, and XRD); writing the original draft. DN: data curation (XAS and XPS) and formal analysis (XPS); writing-review and editing. DD: data curation and formal analysis (XAS); writing-review and editing. ALN: data curation and formal analysis (TEM); writing-review and editing. LB: data curation (XAS); writing-review and editing. BK: data curation and formal analysis (XPS); writing-review and editing. JDG: overall supervision, funding acquisition, resources, writing–discussion–review and editing.

## Conflicts of interest

The authors declare no conflicts of interest.

## Acknowledgements

The authors would like to thank Dr Eduardo Barbosa and Angela Deutsch for nitrogen physisorption measurements and Armin Lautenbach for ICP-OES analysis. Alisa Sinigalia is thanked for her assistance during the XPS measurements. Andrea De Giacinto and Dr Linda Klag are thanked for their assistance with the FSP synthesis. Michael Borchers is thanked for the $H_2$-TPR measurements. Dr Lu Chen (University of Cambridge, UK) and Prof. Philippe Serp (LCC, CNRS, France) are thanked for the fruitful discussion during the preparation of the manuscript. We acknowledge DESY (Hamburg, Germany), a member of the Helmholtz Association HGF, for the provision of beamtime, allocated to the proposals I-20200891 and I-20211473 and KIT light source (A2020-031-018713). We would like to thank Dr Edmund Welter (P65, DESY) and Dr Anna Zimina (CATACT, KIT Light Source and IKFT) for their assistance in setting up the beamline. HAADF-STEM imaging and EDX imaging were carried out with the support of the Karlsruhe Nano Micro Facility (KNMFi, **https://www.knmf.kit.edu**), a Helmholtz Research Infrastructure at the Karlsruhe Institute of Technology (KIT, **https://www.kit.edu**). Support from the Helmholtz Association and Deutsche Forschungsgemeinschaft (DFG, German Research Foundation) – SFB 1441 – Project-ID 426888090 is gratefully acknowledged. BBS would like to thank CNRS for startup funding.

## Notes and references

1 R. Franke, D. Selent and A. Börner, Applied Hydroformylation, *Chem. Rev.*, 2012, **112**, 5675–5732.
2 M. Sparta, K. J. Børve and V. R. Jensen, Activity of Rhodium-Catalyzed Hydroformylation: Added Insight and Predictions from Theory, *J. Am. Chem. Soc.*, 2007, **129**, 8487–8499.
3 P. Forzatti, E. Tronconi and I. Pasquon, Higher Alcohol Synthesis, *Catal. Rev.*, 1991, **33**, 109–168.
4 X. Xiaoding, E. B. M. Doesburg and J. J. F. Scholten, Synthesis of higher alcohols from syngas – recently patented catalysts and tentative ideas on the mechanism, *Catal. Today*, 1987, **2**, 125–170.
5 H. T. Luk, C. Mondelli, D. C. Ferré, J. A. Stewart and J. Pérez-Ramírez, Status and prospects in higher alcohols synthesis from syngas, *Chem. Soc. Rev.*, 2017, **46**, 1358–1426.
6 G. van der Lee, B. Schuller, H. Post, T. L. F. Favre and V. Ponec, On the selectivity of Rh catalysts in the formation of oxygenates, *J. Catal.*, 1986, **98**, 522–529.
7 M. Suvarna, P. Preikschas and J. Pérez-Ramírez, Identifying Descriptors for Promoted Rhodium-Based Catalysts for Higher Alcohol Synthesis *via* Machine Learning, *ACS Catal.*, 2022, **12**, 15373–15385.
8 R. Lang, T. Li, D. Matsumura, S. Miao, Y. Ren, Y. T. Cui, Y. Tan, B. Qiao, L. Li, A. Wang, X. Wang and T. Zhang, Hydroformylation of Olefins by a Rhodium Single-Atom

Catalyst with Activity Comparable to $RhCl(PPh_3)_3$, *Angew. Chem., Int. Ed.*, 2016, **55**, 16054–16058.

9 J. Amsler, B. B. Sarma, G. Agostini, G. Prieto, P. N. Plessow and F. Studt, Prospects of Heterogeneous Hydroformylation with Supported Single Atom Catalysts, *J. Am. Chem. Soc.*, 2020, **142**, 5087–5096.

10 L. Wang, W. Zhang, S. Wang, Z. Gao, Z. Luo, X. Wang, R. Zeng, A. Li, H. Li, M. Wang, X. Zheng, J. Zhu, W. Zhang, C. Ma, R. Si and J. Zeng, Atomic-level insights in optimizing reaction paths for hydroformylation reaction over Rh/CoO single-atom catalyst, *Nat. Commun.*, 2016, **7**, 14036.

11 C. Li, W. Wang, L. Yan and Y. Ding, A mini review on strategies for heterogenization of rhodium-based hydroformylation catalysts, *Front. Chem. Sci. Eng.*, 2018, **12**, 113–123.

12 S. Hanf, L. A. Rupflin, R. Glaser and S. A. Schunk, Current State of the Art of the Solid Rh-Based Catalyzed Hydroformylation of Short-Chain Olefins, *Catalysts*, 2020, **10**, 1–36.

13 X.-F. Yang, A. Wang, B. Qiao, J. Li, J. Liu and T. Zhang, Single-Atom Catalysts: A New Frontier in Heterogeneous Catalysis, *Acc. Chem. Res.*, 2013, **46**, 1740–1748.

14 A. Wang, J. Li and T. Zhang, Heterogeneous single-atom catalysis, *Nat. Rev. Chem.*, 2018, **2**, 65–81.

15 I. Ro, J. Qi, S. Lee, M. Xu, X. Yan, Z. Xie, G. Zakem, A. Morales, J. G. Chen, X. Pan, D. G. Vlachos, S. Caratzoulas and P. Christopher, Bifunctional hydroformylation on heterogeneous Rh-$WO_x$ pair site catalysts, *Nature*, 2022, **609**, 287–292.

16 B. B. Sarma, J. Jelic, D. Neukum, D. E. Doronkin, X. Huang, S. Bernart, F. Studt and J.-D. Grunwaldt, Tracking and Understanding Dynamics of Atoms and Clusters of Late Transition Metals with *In Situ* DRIFT and XAS Spectroscopy Assisted by DFT, *J. Phys. Chem. C*, 2023, **127**, 3032–3046.

17 L. Liu, D. M. Meira, R. Arenal, P. Concepcion, A. V. Puga and A. Corma, Determination of the Evolution of Heterogeneous Single Metal Atoms and Nanoclusters under Reaction Conditions: Which Are the Working Catalytic Sites?, *ACS Catal.*, 2019, **9**, 10626–10639.

18 S. Ding, J. Hülsey Max, H. An, Q. He, H. Asakura, M. Gao, J.-y. Hasegawa, T. Tanaka and N. Yan, Ionic Liquid-Stabilized Single-Atom Rh Catalyst Against Leaching, *CCS Chem.*, 2021, **3**, 1814–1822.

19 G. Zakem and P. Christopher, Active Site Entropy of Atomically Dispersed $Rh/Al_2O_3$ Catalysts Dictates Activity for Ethylene Hydroformylation, *ACS Catal.*, 2023, **13**, 5502–5515.

20 Y. Zheng, Q. Wang, Q. Yang, S. Wang, M. J. Hülsey, S. Ding, S. Furukawa, M. Li, N. Yan and X. Ma, Boosting the Hydroformylation Activity of a $Rh/CeO_2$ Single-Atom Catalyst by Tuning Surface Deficiencies, *ACS Catal.*, 2023, **13**, 7243–7255.

21 L. Qi, S. Das, Y. Zhang, D. Nozik, B. C. Gates and A. T. Bell, Ethene Hydroformylation Catalyzed by Rhodium Dispersed with Zinc or Cobalt in Silanol Nests of Dealuminated Zeolite Beta, *J. Am. Chem. Soc.*, 2023, **145**, 2911–2929.

22 I. Ro, M. Xu, G. W. Graham, X. Pan and P. Christopher, Synthesis of Heteroatom Rh–$ReO_x$ Atomically Dispersed Species on $Al_2O_3$ and Their Tunable Catalytic Reactivity in Ethylene Hydroformylation, *ACS Catal.*, 2019, **9**, 10899–10912.

23 M. Zhao, C. Li, D. Gómez, F. Gonell, V. M. Diaconescu, L. Simonelli, M. L. Haro, J. J. Calvino, D. M. Meira, P. Concepción and A. Corma, Low-temperature hydroformylation of ethylene by phosphorous stabilized Rh sites in a one-pot synthesized Rh-(*O*)-P-MFI zeolite, *Nat. Commun.*, 2023, **14**, 7174.

24 M. Schumann, M. R. Nielsen, T. E. L. Smitshuysen, T. W. Hansen, C. D. Damsgaard, A.-C. A. Yang, M. Cargnello, J.-D. Grunwaldt, A. D. Jensen and J. M. Christensen, Rationalizing an Unexpected Structure Sensitivity in Heterogeneous Catalysis—CO Hydrogenation over Rh as a Case Study, *ACS Catal.*, 2021, **11**, 5189–5201.

25 N. Yang, A. J. Medford, X. Liu, F. Studt, T. Bligaard, S. F. Bent and J. K. Nørskov, Intrinsic Selectivity and Structure Sensitivity of Rhodium Catalysts for $C_{2+}$ Oxygenate Production, *J. Am. Chem. Soc.*, 2016, **138**, 3705–3714.

26 J. J. Spivey and A. Egbebi, Heterogeneous catalytic synthesis of ethanol from biomass-derived syngas, *Chem. Soc. Rev.*, 2007, **36**, 1514–1528.

27 S. R. Foit, I. C. Vinke, L. G. J. de Haart and R.-A. Eichel, Power-to-Syngas: An Enabling Technology for the Transition of the Energy System?, *Angew. Chem., Int. Ed.*, 2017, **56**, 5402–5411.

28 D. Pakhare and J. Spivey, A review of dry ($CO_2$) reforming of methane over noble metal catalysts, *Chem. Soc. Rev.*, 2014, **43**, 7813–7837.

29 W. Sheng, S. Kattel, S. Yao, B. Yan, Z. Liang, C. J. Hawxhurst, Q. Wu and J. G. Chen, Electrochemical reduction of $CO_2$ to synthesis gas with controlled $CO/H_2$ ratios, *Energy Environ. Sci.*, 2017, **10**, 1180–1185.

30 E. Lam and E. Reisner, A $TiO_2$-Co(terpyridine)$_2$ Photocatalyst for the Selective Oxidation of Cellulose to Formate Coupled to the Reduction of $CO_2$ to Syngas, *Angew. Chem., Int. Ed.*, 2021, **60**, 23306–23312.

31 M. He, B. Xiao, Z. Hu, S. Liu, X. Guo and S. Luo, Syngas production from catalytic gasification of waste polyethylene: Influence of temperature on gas yield and composition, *Int. J. Hydrogen Energy*, 2009, **34**, 1342–1348.

32 V. R. Surisetty, A. K. Dalai and J. Kozinski, Alcohols as alternative fuels: an overview, *Appl. Catal., A*, 2011, **404**, 1–11.

33 M. Ao, G. H. Pham, J. Sunarso, M. O. Tade and S. Liu, Active Centers of Catalysts for Higher Alcohol Synthesis from Syngas: A Review, *ACS Catal.*, 2018, **8**, 7025–7050.

34 D. Wu, S. Liu, M. Zhong, J. Zhao, C. Du, Y. Yang, Y. Sun, J. Lin, S. Wan, S. Wang, J. Huang, Y. Yao, Z. Li and H. Xiong, Nature and Dynamic Evolution of Rh Single Atoms Trapped by $CeO_2$ in CO Hydrogenation, *ACS Catal.*, 2022, **12**, 12253–12267.

35 M. Schumann, J.-D. Grunwaldt, A. D. Jensen and J. M. Christensen, Investigations of mechanism, surface species and support effects in CO hydrogenation over Rh, *J. Catal.*, 2022, **414**, 90–100.
36 M. Deimel, H. Prats, M. Seibt, K. Reuter and M. Andersen, Selectivity Trends and Role of Adsorbate–Adsorbate Interactions in CO Hydrogenation on Rhodium Catalysts, *ACS Catal.*, 2022, **12**, 7907–7917.
37 S. M. McClure, M. J. Lundwall and D. W. Goodman, Planar oxide supported rhodium nanoparticles as model catalysts, *Proc. Natl. Acad. Sci. U. S. A.*, 2011, **108**, 931–936.
38 M. Gupta, M. L. Smith and J. J. Spivey, Heterogeneous Catalytic Conversion of Dry Syngas to Ethanol and Higher Alcohols on Cu-Based Catalysts, *ACS Catal.*, 2011, **1**, 641–656.
39 K. Fang, D. Li, M. Lin, M. Xiang, W. Wei and Y. Sun, A short review of heterogeneous catalytic process for mixed alcohols synthesis *via* syngas, *Catal. Today*, 2009, **147**, 133–138.
40 R. G. Herman, Advances in catalytic synthesis and utilization of higher alcohols, *Catal. Today*, 2000, **55**, 233–245.
41 K. Xiao, Z. Bao, X. Qi, X. Wang, L. Zhong, K. Fang, M. Lin and Y. Sun, Advances in bifunctional catalysis for higher alcohol synthesis from syngas, *Chin. J. Catal.*, 2013, **34**, 116–129.
42 D. S. Breslow and R. F. Heck, Mechanism of the Hydroformylation of Olefins, *Chem. Ind.*, 1960, 467.
43 R. F. Heck and D. S. Breslow, The Reaction of Cobalt Hydrotetracarbonyl with Olefins, *J. Am. Chem. Soc.*, 1961, **83**, 4023–4027.
44 S. S. C. Chuang, R. W. Stevens and R. Khatri, Mechanism of $C_{2+}$ oxygenate synthesis on Rh catalysts, *Top. Catal.*, 2005, **32**, 225–232.
45 S. S. C. Chuang and S. I. Pien, Infrared study of the CO insertion reaction on reduced, oxidized, and sulfided Rh/$SiO_2$ catalysts, *J. Catal.*, 1992, **135**, 618–634.
46 H. Xiong, S. Lin, J. Goetze, P. Pletcher, H. Guo, L. Kovarik, K. Artyushkova, B. M. Weckhuysen and A. K. Datye, Thermally Stable and Regenerable Platinum–Tin Clusters for Propane Dehydrogenation Prepared by Atom Trapping on Ceria, *Angew. Chem., Int. Ed.*, 2017, **56**, 8986–8991.
47 M. Akri, S. Zhao, X. Li, K. Zang, A. F. Lee, M. A. Isaacs, W. Xi, Y. Gangarajula, J. Luo, Y. Ren, Y.-T. Cui, L. Li, Y. Su, X. Pan, W. Wen, Y. Pan, K. Wilson, L. Li, B. Qiao, H. Ishii, Y.-F. Liao, A. Wang, X. Wang and T. Zhang, Atomically dispersed nickel as coke-resistant active sites for methane dry reforming, *Nat. Commun.*, 2019, **10**, 5181.
48 B. B. Sarma, G. Agostini, M. G. Farpón, C. Marini, N. Pfänder and G. Prieto, Bottom-up assembly of bimetallic nanocluster catalysts from oxide-supported single-atom precursors, *J. Mater. Chem. A*, 2021, **9**, 8401–8415.
49 J. C. Matsubu, V. N. Yang and P. Christopher, Isolated Metal Active Site Concentration and Stability Control Catalytic $CO_2$ Reduction Selectivity, *J. Am. Chem. Soc.*, 2015, **137**, 3076–3084.
50 A. Aitbekova, L. Wu, C. J. Wrasman, A. Boubnov, A. S. Hoffman, E. D. Goodman, S. R. Bare and M. Cargnello, Low-Temperature Restructuring of $CeO_2$-Supported Ru Nanoparticles Determines Selectivity in $CO_2$ Catalytic Reduction, *J. Am. Chem. Soc.*, 2018, **140**, 13736–13745.
51 J.-D. Grunwaldt, L. Basini and B. S. Clausen, *In Situ* EXAFS Study of Rh/$Al_2O_3$ Catalysts for Catalytic Partial Oxidation of Methane, *J. Catal.*, 2001, **200**, 321–329.
52 J. Jones, H. Xiong, A. T. DeLaRiva, E. J. Peterson, H. Pham, S. R. Challa, G. Qi, S. Oh, M. H. Wiebenga, X. I. Pereira Hernández, Y. Wang and A. K. Datye, Thermally stable single-atom platinum-on-ceria catalysts *via* atom trapping, *Science*, 2016, **353**, 150.
53 B. B. Sarma, J. Kim, J. Amsler, G. Agostini, C. Weidenthaler, N. Pfänder, R. Arenal, P. Concepción, P. Plessow, F. Studt and G. Prieto, One-Pot Cooperation of Single-Atom Rh and Ru Solid Catalysts for a Selective Tandem Olefin Isomerization–Hydrosilylation Process, *Angew. Chem., Int. Ed.*, 2020, **59**, 5806–5815.
54 C. Galdeano-Ruano, C. W. Lopes, D. Motta Meira, A. Corma and P. Oña-Burgos, Rh2P Nanoparticles Stabilized by Carbon Patches for Hydroformylation of Olefins, *ACS Appl. Nano Mater.*, 2021, **4**, 10743–10753.
55 R. Koirala, S. E. Pratsinis and A. Baiker, Synthesis of catalytic materials in flames: opportunities and challenges, *Chem. Soc. Rev.*, 2016, **45**, 3053–3068.
56 B. B. Sarma and J.-D. Grunwaldt, *Operando* Spectroscopy to Understand Dynamic Structural Changes of Solid Catalysts, *Chimia*, 2024, **78**, 288–296.
57 B. B. Sarma, F. Maurer, D. E. Doronkin and J.-D. Grunwaldt, Design of Single-Atom Catalysts and Tracking Their Fate Using *Operando* and Advanced X-ray Spectroscopic Tools, *Chem. Rev.*, 2023, **123**, 379–444.
58 G. Cavusoglu, D. Miao, H. Lichtenberg, H. W. P. Carvalho, H. Xu, A. Goldbach and J.-D. Grunwaldt, Structure and activity of flame made ceria supported Rh and Pt water gas shift catalysts, *Appl. Catal., A*, 2015, **504**, 381–390.
59 V. Muravev, G. Spezzati, Y.-Q. Su, A. Parastaev, F.-K. Chiang, A. Longo, C. Escudero, N. Kosinov and E. J. M. Hensen, Interface dynamics of Pd–$CeO_2$ single-atom catalysts during CO oxidation, *Nat. Catal.*, 2021, **4**, 469–478.
60 W. J. Stark, J.-D. Grunwaldt, M. Maciejewski, S. E. Pratsinis and A. Baiker, Flame-Made Pt/Ceria/Zirconia for Low-Temperature Oxygen Exchange, *Chem. Mater.*, 2005, **17**, 3352–3358.
61 J. Finzel, K. M. Sanroman Gutierrez, A. S. Hoffman, J. Resasco, P. Christopher and S. R. Bare, Limits of Detection for EXAFS Characterization of Heterogeneous Single-Atom Catalysts, *ACS Catal.*, 2023, **13**, 6462–6473.
62 L. Basini, M. Marchionna and A. Aragno, Drift and mass spectroscopic studies on the reactivity of rhodium clusters at the surface of polycrystalline oxides, *J. Phys. Chem.*, 1992, **96**, 9431–9441.
63 F. C. Meunier, Relevance of IR Spectroscopy of Adsorbed CO for the Characterization of Heterogeneous Catalysts Containing Isolated Atoms, *J. Phys. Chem. C*, 2021, **125**, 21810–21823.
64 Y. Kwon, T. Y. Kim, G. Kwon, J. Yi and H. Lee, Selective Activation of Methane on Single-Atom Catalyst of Rhodium

Dispersed on Zirconia for Direct Conversion, *J. Am. Chem. Soc.*, 2017, **139**, 17694–17699.

65 B. B. Sarma, P. N. Plessow, G. Agostini, P. Concepción, N. Pfänder, L. Kang, F. R. Wang, F. Studt and G. Prieto, Metal-Specific Reactivity in Single-Atom Catalysts: CO Oxidation on 4d and 5d Transition Metals Atomically Dispersed on MgO, *J. Am. Chem. Soc.*, 2020, **142**, 14890–14902.

66 A. M. Beale and B. M. Weckhuysen, EXAFS as a tool to interrogate the size and shape of mono and bimetallic catalyst nanoparticles, *Phys. Chem. Chem. Phys.*, 2010, **12**, 5562–5574.

67 D. A. J. M. Ligthart, R. A. van Santen and E. J. M. Hensen, Influence of particle size on the activity and stability in steam methane reforming of supported Rh nanoparticles, *J. Catal.*, 2011, **280**, 206–220.